# Rhodium nanoparticles stabilized by ferrocenyl-phosphine ligands: synthesis and catalytic styrene hydrogenation

Mona Ibrahim, M. Wei, Éric Deydier, E. Manoury, Rinaldo Poli, Pierre
Lecante, Karine Philippot

# Rhodium nanoparticles stabilized by ferrocenyl-phosphine ligands: synthesis and catalytic styrene hydrogenation.

M. Ibrahim,[1,2] , M. M. Wei,[1,2] E. Deydier,[1,2,3]* E. Manoury,[1,2]* R. Poli[1,2] P. Lecante[4] and K. Philippot[1,2]*

1) CNRS, LCC (Laboratoire de Chimie de Coordination), 205, route de Narbonne, BP 44099, F-31077 Toulouse cedex 4, France
2) Université de Toulouse, UPS, INPT, F-31077 Toulouse cedex 4, France
3) IUT A Paul Sabatier, Département de Chimie, Avenue Georges Pompidou, CS 20258, F-81104 Castres Cedex, France
4) CNRS, CEMES (Centre d'Elaboration de Matériaux et d'Etudes Structurales), 29 rue J. Marvig, F-31055 Toulouse, France

## Graphical abstract

A series of ferrocenyl-phosphine ligands has been used to stabilize small rhodium nanoparticles that are active in the catalytic hydrogenation of styrene.

**Abstract**

A series of ferrocenylphosphine-stabilized rhodium nanoparticles has been prepared in one pot from the organometallic [Rh($\eta^3$-C$_3$H$_5$)$_3$] precursor. This complex has been decomposed by hydrogen treatment (3 bar) in dichloromethane in the presence of five different ferrocene-based phosphine ligands. Very small rhodium nanoparticles in the size range of 1.1-1.7 nm have been obtained. These nanoparticles have shown activity in a model catalytic reaction, namely the hydrogenation of styrene. These results evidence that the metal surface is not blocked despite the steric bulk of the stabilizing ligands. Moreover, certain selectivity has been observed depending on the ligand employed. To our best knowledge, such type of compounds has not been yet used for stabilizing metal nanoparticles and our findings highlight the interest to do so.

**Key-words**

**Introduction**

Metal nanoparticles (NPs) are largely investigated given their unique properties and potential applications in multiple domains such as biology, medicine, microelectronics, optics or catalysis to cite only a few.[1,2,3] In catalysis, the relevance of metal NPs has been known for a long time due to their presence in heterogeneous catalysts.[4,5] Metal NPs are attractive materials because of their high surface/volume ratio.[6,7] With the recent advances in nanochemistry and particularly in the design of better defined metal NPs, nanocatalysis is now recognized as a full and rich part of catalysis.[8,9,10]

During the past 25 years ligand-stabilized metal nanoparticles have attracted growing attention and numerous investigations are devoted to exploring the effect of the stabilizing agents on the characteristics of NPs such as size, dispersion, morphology and surface properties or also catalytic performance.[11] Very recent papers reported on the precise role of ligands and their binding with the metal surface on the NP size control.[12,13] It is important to note that the interaction of the ligands with the metal atoms on the NP surface can be

compared to the ligand interaction with the metal centers in homogeneous catalysts, which is of paramount importance for stability and properties like catalytic activity. Thus, ligands also allow tuning the surface properties of metal NPs through electronic or steric effects. Moreover, ligand-stabilized metal nanoparticles can be applied to catalysis either as stable colloidal suspensions or after deposition on the surface or confinement in the pores of solid supports.[14] The challenge is to find ligands able to stabilize well-defined nanoparticles while controlling accessibility at the metal surface and reactivity.[15] Compared to the investigation of facet dependency, the ligand influence on the catalytic activity has been less intensively studied but recent results illustrate well the interest to do so.[16,17,18,19] One aim lies on the design of more performing catalysts in terms of reactivity and selectivity in order to develop more efficient and eco-compatible chemical production.[20]

One efficient method to prepare well-controlled metal nanoparticles is the organometallic approach. This approach has proven powerful to provide controlled nanoparticles with reproducible physical or chemical properties.[21] Metal complexes (organometallic or metal organic complexes) are decomposed under mild conditions to release metal atoms either in the presence of polymers (steric barriers) or ligands (metal surface coordination) as stabilizing agents. The choice of the metal source is important in terms of the resulting metal surface purity. Olefinic metal precursors are privileged because their treatment under hydrogen liberates alkanes as the only reaction byproducts that are inert towards the metal surface. So, metal NPs with clean surfaces capped with the desired ligands are obtained. Numerous ruthenium nanoparticles have been prepared this way, using $[Ru(\eta^6\text{-}C_8H_{10})((\eta\text{-}C_8H_{12})]$ as ruthenium source and a large panel of ligands as stabilizers. The ligands are either simple or sophisticated, and mainly contain amines, thiols, carbenes or phosphines that were shown to influence the surface and the catalytic properties of the particles.[22]

Rhodium particles can also be synthesized by the organometallic method, starting from $[Rh(acac)(1,5\text{-}C_8H_{12})],$[23] $[Rh(\mu Cl)(1,5\text{-}C_8H_{12})]_2$[24], or $[Rh(\eta^3\text{-}C_3H_5)_3].$[25] Phosphines ligands were shown to affect the reactivity of Rh NPs in hydrogenation[26,27] and hydroformylation catalysis.[28] Apart from usual ligands to stabilize metal NPs, one can envisage to use metal-containing ligands. This can be of interest in order to introduce novel properties like redox surface modulation and also more functionality.[29,30] One application could be tandem catalysis for instance. One strategy to achieve this objective is to consider metal-containing ligands with functional groups able to interact with the metal surface such as phosphine
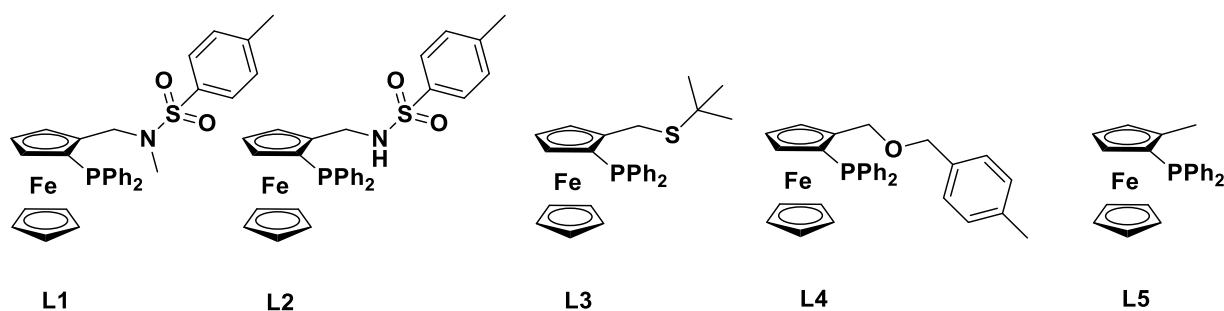
groups.[31]  To this end, we chose to test ferrocene-based phosphine ligands because these compounds have several attractive properties: they are stable, they may feature planar chirality with potential interest in materials chemistry[32]  and especially in asymmetric catalysis,[33,34,35]  and they possess a redox-active ferrocene moiety which may be exploited for switchable catalysis.[36,37,38] For instance, 1,2-disubstituted ferrocene phosphines play a major role in several asymmetric catalysis applications. Various examples including bidendate (P,P),[39] (P,N),[40] (P,S),[41,42,43] (P,O)[44,45,46,47] and (P, carbene)[48] compounds have been reported, illustrating the great modularity of this family of ligands. To our best knowledge there is no previous example of the use of such ligands for the stabilization of metal nanoparticles.

In the present work we have focused on a series of racemic ferrocenylphosphine ligands as stabilizing agents for rhodium nanoparticles obtained by a one-pot synthesis from $[Rh(\eta^3\text{-}C_3H_5)_3]$. As it will be described hereafter, a series of small rhodium nanoparticles in a size range between 1.1 and 1.7 nm have been obtained and these were shown to be active for a model catalytic reaction, namely the hydrogenation of styrene.
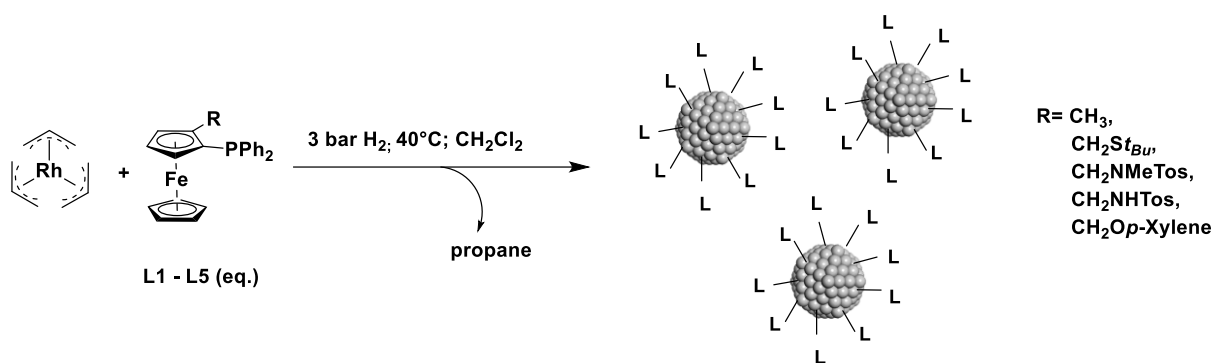

**Results and discussion**

The first objective of this work was to take benefit of previous results in the organometallic synthesis of phosphine-stabilized rhodium nanoparticles, achieved from the $[Rh(\eta^3\text{-}C_3H_5)_3]$ complex as metal source and simple mono- or di-substituted phosphines as stabilizers,[26,28] in order to prepare a new family of Rh NPs by the same approach but using ferrocenyl phosphines. With ferrocene-based-phosphine-capped Rh NPs in hands, a second objective was to test their catalytic activity in a benchmark hydrogenation process, the hydrogenation of styrene, in order to evaluate the influence of the capping ligands at the rhodium surface.

All the ligands employed in this study (Scheme 1) are ferrocenyl diphenyl phosphines bearing different substituted methyl groups at the 2 position. **L1** and **L2** are both P,N bidentate ligands.[49] In **L1** the amine is tertiary with an extra methyl substituent on the nitrogen atom, whereas **L2** contains a secondary amine. Ligand **L3**[50]  and **L4**[35c] are respectively P,S and P,O bidendate ligands. **L5** is the simplest ligand of the series, the only monodentate one, having a methyl group at the ferrocenyl 2 position.

The synthesis of the NPs was performed in one pot using dichloromethane ($CH_2Cl_2$) as the solvent in order to insure the solubility of both the [Rh($\eta^3$-$C_3H_5$)$_3$] complex and the ferrocenyl phosphine ligands. Thus, a Fischer-Porter reactor filled with a $CH_2Cl_2$ solution containing both [Rh($\eta^3$-$C_3H_5$)$_3$] and a given ferrocenyl ligand was pressurized with 3 bar of dihydrogen and then heated at 40°C, under vigorous stirring (Scheme 2). A change of color from a yellow homogeneous solution to a black colloidal suspension was observed over a few hours of stirring, but the reaction was kept running up to 16 h to insure a complete decomposition of the precursor and the formation of a homogeneous population of particles. For the four ligands **L1**, **L2**, **L3** and **L4,** a [ligand]/[Rh] ratio of 0.2 molar equivalent was used**.** These ligands being bidentate, they offer an extra coordination through the second donor group, for an effective [donor]/[metal] ratio of 0.4. For ligand **L5**, which is monodentate, a molar [ligand]/[Rh] ratio of 0.4 was applied for comparison purpose. These [ligand]/[Rh] ratios appeared to be sufficient to yield stable colloidal suspensions for several weeks under an argon atmosphere. This is particularly important to note when considering that the **L5** ligand has only one –$PPh_2$ coordinating group. Indeed, when $PPh_3$ was used as a stabilizer, a minimum [ligand]/[Rh] ratio of 1 was necessary to reproducibly yield stable colloidal suspensions of small Rh NPs (ca. 1.3 nm).[26] For comparison, the bidentate $Ph_2P$-$(CH_2)_4$-$PPh_2$ ligand led to stable Rh NPs at a [ligand]/[Rh] ratio of 0.3 molar equivalent, which amounts to a [donor]/[Rh] ratio of 0.6. Consequently, the bidendate phosphino-ferrocenyl ligands used here behave as efficient stabilizers at lower [ligand]/[Rh] ratios compared to the previously studied similar mono- and diphosphane ligands. The purification of the particles was performed by precipitation after addition of cold pentane to the concentrated colloidal suspensions. The generated black precipitates were isolated by decanting off the solvents, washing and drying under vacuum, leading to dried nanoparticle powders.

**Scheme 2**: On-pot synthesis of ferrocenylphosphine-capped Rh NPs

TEM images recorded from samples prepared by deposition of a few drops of the crude colloidal suspensions onto a carbon-covered copper grid showed well-dispersed NPs for all the systems studied. They present spherical shapes and quite narrow size distributions, in a size range between 1 and 2 nm (Figure 1), with mean diameters as follows: $1.5 \pm 0.6$ nm for Rh@**L1** NPs, $1.7 \pm 0.5$ nm for Rh@**L2** NPs, $1.3 \pm 0.7$ nm for Rh@**L3** NPs =, $1.1 \pm 0.5$ nm for Rh@**L4** NPs, and $1.2 \pm 0.6$ nm for Rh@**L5** NPs.
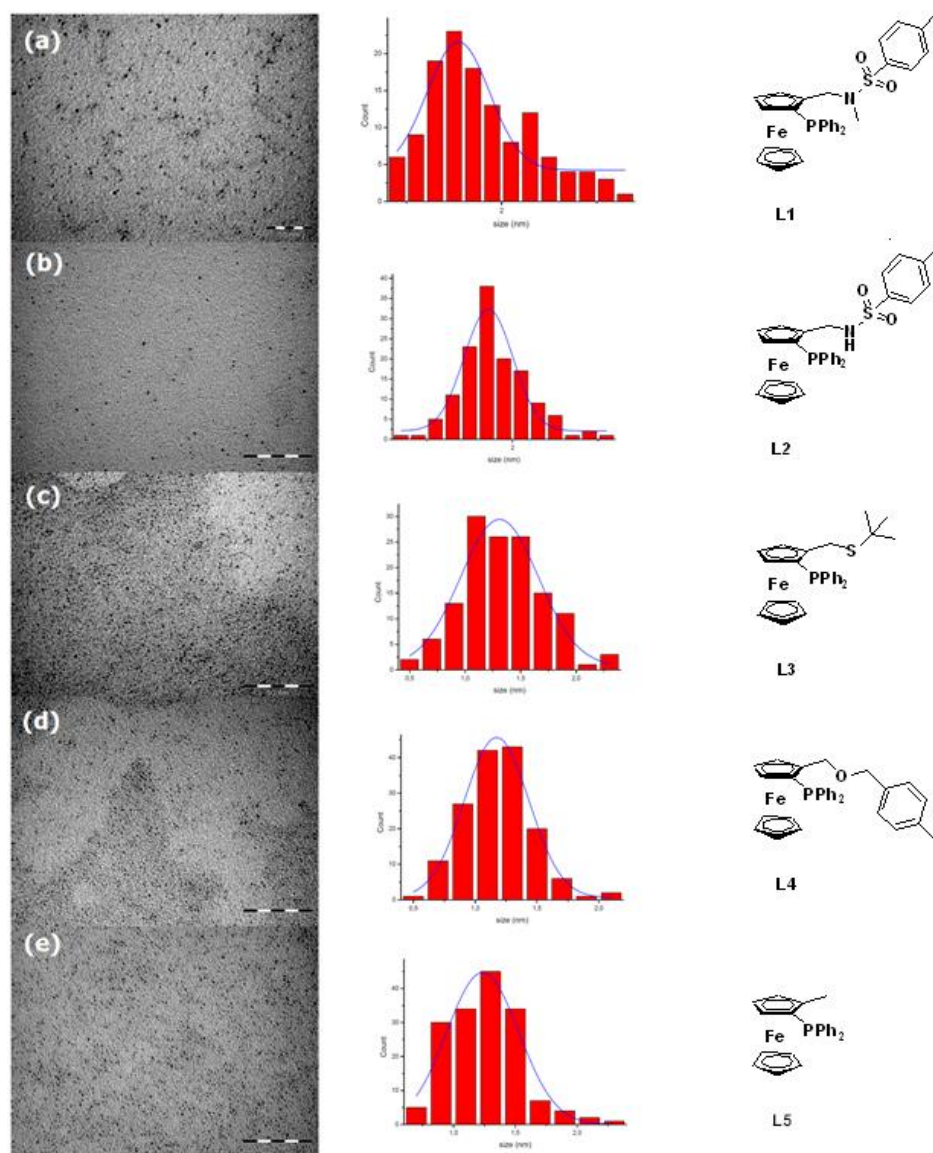
**Figure 1:** (a) TEM images and corresponding size distributions of Rh NPs stabilized with **L1**, (b) **L2**, (c) **L3**, (d) **L4**, (e) **L5**.

The **L2-** and **L5**-stabilized nanoparticles were investigated in greater details in order to learn more about the effect of a second donor function. Thus, Rh@**L2** NPs and Rh@**L5** NPs were also characterized by high resolution electron microscopy (HREM). In addition to isolated nanoparticles, the HREM images of the **L2-**stabilized Rh NPs also revealed the presence of large agglomerates (Figure 2 top), which appeared composed of small and spherical particles gathered together. The isolated particles displayed crystalline regions with interplanar distances of 0.22 nm, in good agreement with the fcc structure (face-centered cubic) previously observed for similarly made Rh nanoparticles and for bulk rhodium.[26]  In the case of **L5**-stabilized Rh NPs no agglomerates were observed besides isolated NPs. These latter

7

were poorly crystallized with only a few of them displaying crystalline plans. Moreover Rh-Rh distances measured did not fit perfectly with the fcc crystalline structure as for the bulk rhodium (Figure 2 bottom). Such a phenomenon was previously observed for PPh₃-stabilized RhNPs and explained as the result of a strong coordinating effect of the phosphine ligand.[26]
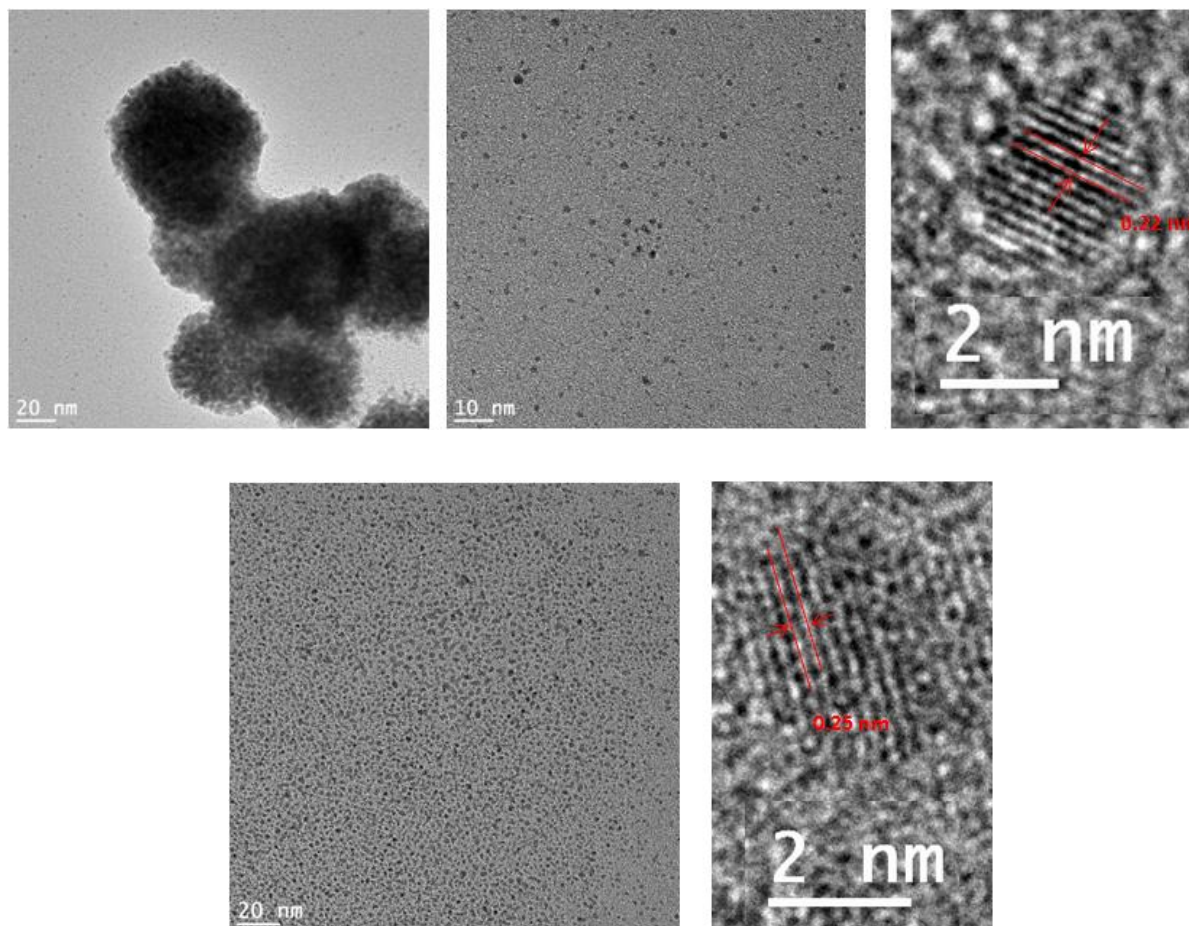


**Figure 2**: HREM images of **L2**-stabilized Rh NPs (top) and **L5**-stabilized Rh NPs (bottom) at different magnifications.

For the Rh@**L2** powder, WAXS (Wide-Angle X-ray Scattering) data revealed well-crystallized particles and confirmed their fcc crystalline structure as for the bulk metal. From the RDF, coherence length reached 3.5-4.0 nm, much more than the average diameter of ca. 1.7 ± 0.5 nm determined from the TEM images (Figure 3 top). However, the envelope of the RDF, related to the size and shape of the objects, is not consistent with single-size spherical NPs but suggests a mixture with a majority of relatively small NPs (ca. 2.0 nm) and a small proportion of much larger ones (up to 4.0 nm). This may be related to a partial coalescence of the small NPs occurring in the agglomerated parts of the sample. For the Rh@**L5** sample (Figure 3 bottom), the RDF indicated a much smaller coherence length of ca. 1.3 nm, which is

in good agreement with the size measured by TEM (1.2 ± 0.6 nm). These particles, however, appeared less crystalline and displayed in reciprocal space a pattern much different from the fcc network, but in good agreement with the manganese-β structure (ICSD 41775, PDF 33-887) already observed for very small Rh NPs[26,51]. These WAXS results suggest that ligand **L5** has a stronger influence than ligand **L2** on the crystallization state of the particles.
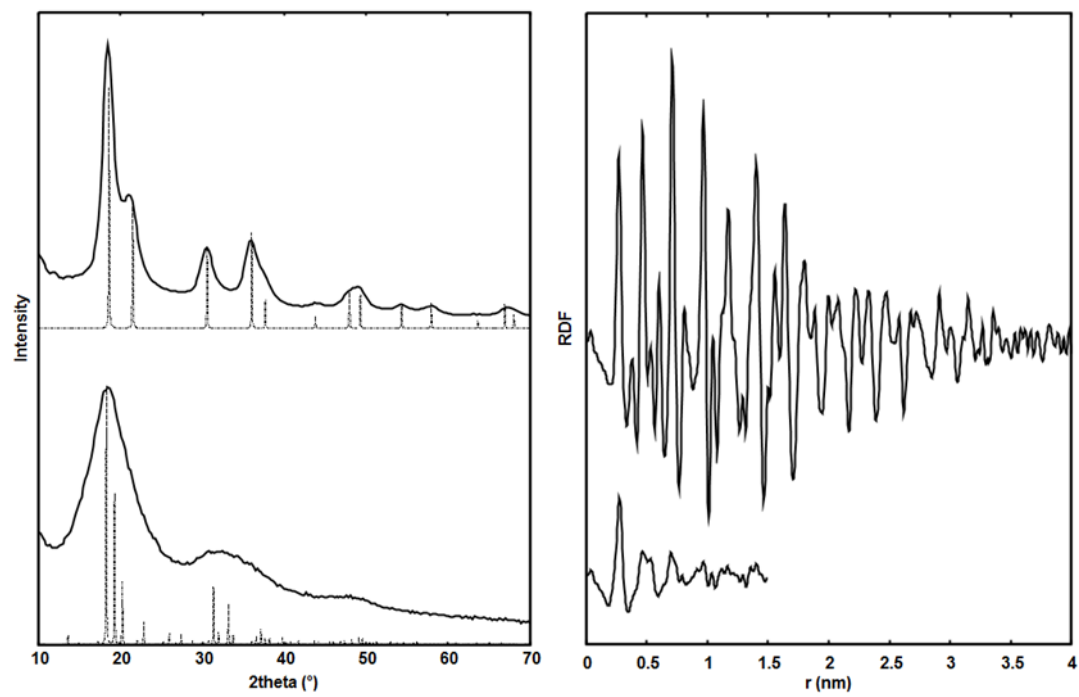


**Figure 3**: WAXS measurements (solid line) for **L2**-stabilized Rh NPs (top) and **L5**-stabilized Rh NPs (bottom) in reciprocal space (left, with reference diagrams for Rh in the fcc and manganese-β structures, dashed line) and real space (right)

Purified samples of **L2-** and **L5-**stabilized Rh NPs were also analyzed by Fourier transform infrared (FT-IR) spectroscopy before and after exposure to a CO atmosphere (1 bar; 48h) in the solid state. This investigation provided information on the coordination ability of CO molecules on the rhodium surface. Similar analyses were previously reported for Ru[52] and Rh[53] NPs. The obtained spectra (KBr pellets) are given in figures 4 and 5 for the **L2-** and **L5-**stabilized Rh NPs, respectively.

In the case of Rh@**L5** NPs, the FT-IR spectrum recorded after 48h of reaction with CO (Figure 4b) revealed the presence of complex bands in the region between 2050 cm^{-1} and 1550

9

cm$^{-1}$ in addition to those already present before CO exposure (Figure 4a). The large and intense band at ca. 1990 cm$^{-1}$ can be attributed to the stretching vibration of CO ligands adopting a terminal coordination mode. The higher frequency shoulder at ca. 2020 cm$^{-1}$ is attributable to the CO ligands bonded in a geminal or multicarbonyl mode. Finally the band at 1800 cm$^{-1}$ can be attributed to the standard bridging coordination mode. The high intensity of the band at 1990 cm$^{-1}$ indicates that terminal CO molecules are abundant. It is generally accepted that this type of coordination occurs on the edges and corners of the particle surface while the bridging coordination mode happens on the extended faces of the particles.[54,55] Given that ligand **L5** allows the CO coordination in all possible coordination modes and that the quantity of terminal CO is high, one can conclude that the metal surface remains relatively accessible with this ligand.



**Figure 4**: (a) FT-IR spectrum of **L5**-stabilized Rh NPs (b) FT-IR spectrum of **L5**-stabilized Rh NPs after 48h under 1 bar of CO.

Conversely, exposure of Rh@**L2** to CO yields only one new and very low intensity band at 1924 cm$^{-1}$ (Figure 5), suggesting a much more limited access for the CO molecules to the metal surface in this case. This effect may result from a tighter **L2** coordination, probably induced by the bidentate character of **L2** and possibly also by a larger covering of the particle surface by **L2** relative to **L5**.
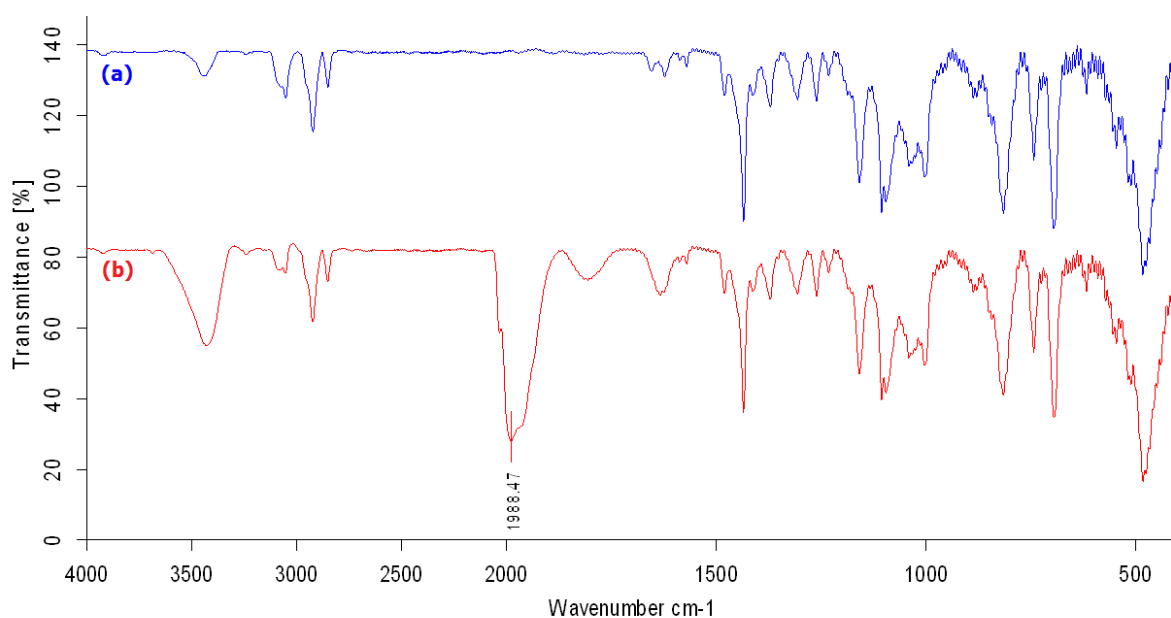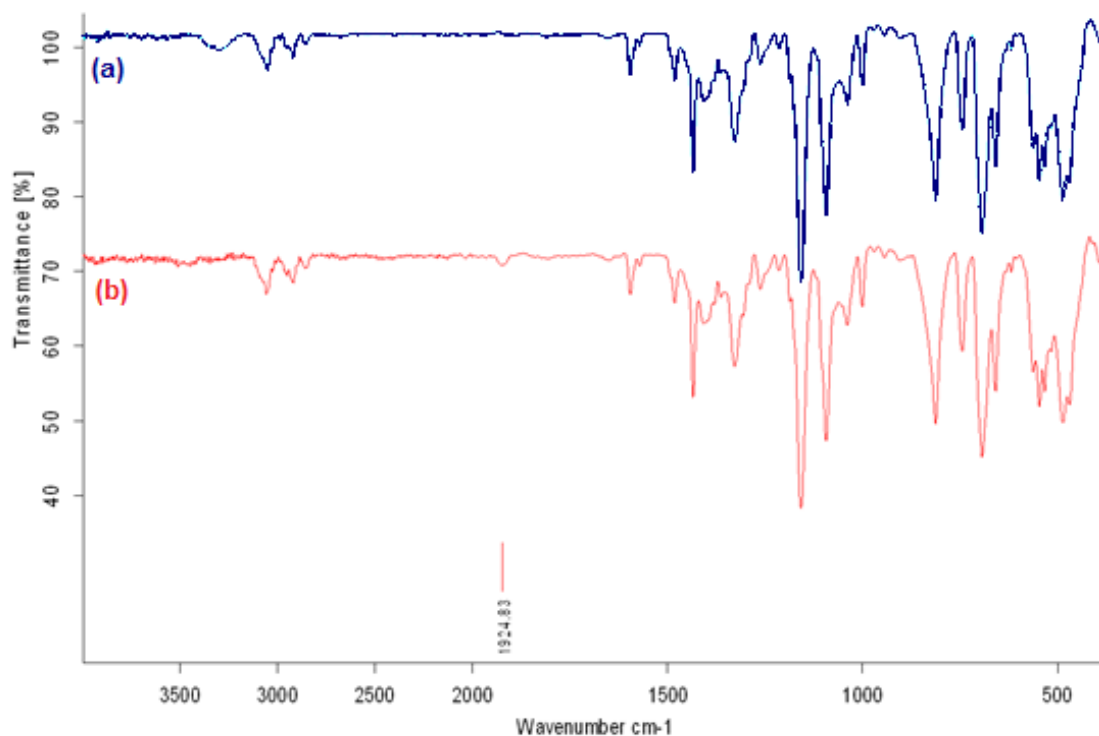
**Figure 5**: (a) FT-IR spectrum of purified **L2**-stabilized Rh NPs (b) FT-IR spectrum of **L2**-stabilized Rh NPs after 48h under 1 bar of CO.

In summary, the FT-IR data suggest that **L2** ligand has a stronger steric effect on the RhNPs surface covering than **L5** one. This can be attributed to the different coordination modes at the NP surface which can result from the different bonding mode (bidentate vs. monodentate). Consequently, a greater fraction of Rh free sites are probably available in the case of Rh@**L5** NPs than in the case of Rh@**L2** NPs.

Rhodium nanoparticles stabilized with ligands **L2** and **L5** were then evaluated in the catalytic hydrogenation of styrene, in order to assess the ligand effect in this simple model reaction. Hydrogenation reactions were performed at room temperature in an autoclave under a 30-bar $H_2$ pressure, using isopropanol as a solvent. The activity was determined by GC analysis after 24 h of reaction. The obtained results are summarized in Table 1.

In all cases, the styrene substrate reached full conversion. In the absence of base and with a 0.7% or 0.2% molar percent of **L2**-stabilized Rh NPs (entries 1 and 2, respectively), ethylbenzene (P1) was the major product but formation of the complete hydrogenation product (ethylcyclohexane, P2) was also observed. The ethylcyclohexane yield increased

11

from 2 to 8 % by increasing the catalyst loading from 0.2 to 0.7 mol. %. The putative product of selective arene hydrogenation, vinylcyclohexane, was never observed. These results suggest a sequential reaction with initial reduction of the vinyl function to ethylbenzene, followed by a slower arene ring reduction to ethylcyclohexane. To confirm this hypothesis, an independent ethyl benzene reduction was carried out under similar conditions (entry 5), yielding 6 % of P2 (similar to the results obtained in entry 1). These reactions were repeated in the presence of excess NaOMe (7-8 equivalents relative to Rh, entries 3, 4 and 6). While the styrene consumption remained complete, the formation of the total reduction product P2 was no longer observed. Thus, the base prevents the arene hydrogenation favoring the selective formation of ethylbenzene (P1).

Similar results were observed when using the **L5**-stabilized Rh NPs. Reactions performed with 0.4 and 0.1 molar % of Rh (entries 7 and 8) gave 10% and 3% of the fully hydrogenated product (P2), and 90% and 97% of ethylbenzene (P1), respectively. The P2 yield increased at higher catalyst loading, as observed with the **L2**-stabilized Rh NPs. When NaOMe was added (entry 9 and 10) the P2 yield dramatically decreased.

A comparison of entries 5 and 11 shows that Rh@**L5** has a greater activity than Rh@**L2** for the arene ring hydrogenation, which can be correlated with the FT-IR suggestion of a more accessible surface for the former catalyst. Deeper mechanistic investigations will be necessary to understand how the presence of the base prevents the arene reduction.

**Table 1**: Styrene and ethyl-benzene hydrogenation using **L2**- and **L5**-stabilized Rh NPs under 30 bar of $H_2$ at R.T.



| Entry | Catalyst | Substrate | $n_{Substrate}$ | S/C$^a$ | Catalyst (%)$^b$ | $n_{base}/n_{Rh}$ | Styrene (%) | P1 (%) | P2 (%) | TON |
|-------|----------|-----------|-----------------|---------|------------------|-------------------|-------------|--------|--------|-----|
| 1 | | Styrene | 0.0005 | 146 | 0.7 | 0 | 0 | 92 | 8 | 146 |
| 2 | | Styrene | 0.0015 | 439 | 0.2 | 0 | 0 | 98 | 2 | 439 |
| 3 | **L2 Rh NPs** | Styrene | 0.0005 | 146 | 0.7 | 7 | 0 | > 99 | < 1 | 146 |
| 4 | | Styrene | 0.0015 | 439 | 0.2 | 8 | 0 | > 99 | < 1 | 439 |
| 5 | | Ethyl-benzene | 0.0005 | 144 | 0.7 | 0 | -- | 94 | 6 | 144 |
| 6 | | Ethyl-benzene | 0.0005 | 144 | 0.7 | 7 | -- | > 99 | < 1 | 144 |
| 7 | | Styrene | 0.0005 | 252 | 0.4 | 0 | 0 | 90 | 10 | 252 |
| 8 | | Styrene | 0.0015 | 756 | 0.1 | 0 | 0 | 97 | 3 | 756 |
| 9 | **L5 Rh NPs** | Styrene | 0.0005 | 252 | 0.4 | 14 | 0 | 98 | 2 | 252 |
| 10 | | Styrene | 0.0015 | 756 | 0.1 | 16 | 0 | > 99 | < 1 | 756 |
| 11 | | Ethyl-benzene | 0.0005 | 247 | 0.4 | 0 | -- | 81 | 19 | 247 |
| 12 | | Ethyl-benzene | 0.0005 | 247 | 0.4 | 15 | -- | 99 | 1 | 247 |

**a**: substrate to rhodium molar ratio.   **b**: mol. %.

**Conclusion**

Ferrocene-based ligands, namely ferrocenyldiphenylphosphines, have been here reported for the first time as stabilizers for the synthesis of metal nanoparticles. The Rh nanoparticles formed with these ligands have a well-controlled size and are quite small (1-2 nm range). The FT-IR study after exposure to a CO atmosphere has shown that the surface covering effect of the bidentate **L2** ligand is greater than that of the monodentate **L5** ligand. These NPs were found catalytically active in the hydrogenation of a model substrate, namely styrene, under very mild reaction conditions in spite of the surface coverage by the ligands. In addition, we have discovered that NaOMe greatly inhibits the hydrogenation of the phenyl ring. This inhibition is, to the best of our knowledge, unprecedented. No significant differences in selectivity were observed using mono- and bidentate ligands, but the NPs stabilized by the monodentate ligand **L5** are more active than those stabilized by the bidentate ligand **L2** in arene hydrogenation of ethylbenzene, in accordance with the lower efficiency of **L5** to cover the nanoparticle surface. Deeper investigations will be necessary for a better understanding of the reaction mechanism and product selectivity.

**Conflict of interest**

There are no conflicts of interest to declare.

**Experimental part**

**1. General and Materials**

Chemicals were purchased as follows: dichoromethane ($CH_2Cl_2$) and pentane from SDS; $RhCl_3.xH_2O$ from Johnson Matthey; [$CH_2=CHCH_2MgCl$], $P(NMe_2)_3$ and $BH_3 \cdot THF$ (1 M solution in THF) from Sigma Aldrich ; $H_2$ from Air Liquide. Solvents were purified before use by filtration on an adequate column of a MBraun purification apparatus and handled under argon atmosphere.

All reagents were used without purification. Reagents and solvents were degassed before use according to a freeze-pump-thaw process. All operations concerning the synthesis of Rh precursor and Rh nanoparticles or the preparation of samples for characterization were carried out using standard Schlenk tubes and Fischer-Porter bottle techniques or in a glove-box (MBraun) under argon atmosphere.

## 2. Characterization techniques

**Transmission electron microscopy** observations at low (TEM) and high resolution (HREM) were performed at the "Centre de microcaractérisation Raymond Castaing" in Toulouse (UMS-CNRS 3623). TEM grids were prepared by drop-casting of the crude colloidal suspension in $CH_2Cl_2$ onto a holey carbon-coated copper grid under argon atmosphere inside a glove-box. TEM images were obtained using either a JEOL 1100 electron microscope operating at 100 kV with point resolution of 4.5 Å or a JEOL JEM 1400 operating at 120 kV with point resolution of 4.5 Å. HTEM observations were carried out with a JEOL JEM 2010 electron microscope working at 200 kV with a point resolution of 2.3 Å and equipped with EDS (Energy Dispersive X-ray Spectroscopy) mode. Statistical size distributions were built by analyzing TEM images with Image J tool software, counting mean diameters of > 200 non-touching particles and assuming a spherical form. Size distributions are quoted as the mean diameter ± the double of the standard deviation (σ) which corresponds to a 95% confidence level. Fourier Fast Transform treatments were carried out with Digital Micrograph Software (Version 1.80.70).

**Wide-angle X-ray scattering (WAXS)** measurements were performed at the CEMES-CNRS in Toulouse. Samples in the solid state were sealed in 1.5 mm diameter Lindemann glass capillaries. The samples were irradiated with graphite monochromatized molybdenum Kα (0.071069 nm) radiation and the X-ray scattering intensity measurements were performed using a dedicated two-axis diffractometer. Radial distribution functions (RDF) were obtained after Fourier transformation of the corrected and reduced data.

**Infrared Spectroscopy**

Fourier Transform Infrared (FT-IR) spectra of **L2-** and **L5-**stabilized RhNPs were recorded in the range 4000-400 cm$^{-1}$ under argon atmosphere using a Perkin-Elmer GX2000 spectrometer installed inside a glovebox. First, the spectra of the purified NPs (KBr pellets prepared in the glove box) were recorded. Second, powders of puridied nanoparticles were exposed under CO atmosphere (1 bar ; 48h) inside a Fischer porter reactor. After evacuation of excess CO, novel FT-IR spectra were recorded (KBr pellets).

**ICP OES and elemental analysis**

ICP OES analyses were performed at the "Service d'analyse élémentaire" of LCC-CNRS in Toulouse using Thermo Scientific iCAP 6300 DUO spectrometer with a 3-channel, 12-roller pump, and a 27.12 MHz solid state RF plasma generator. Mineralization of the NPs was performed in a refluxing aqua regia solution.

**3. Synthesis methods**
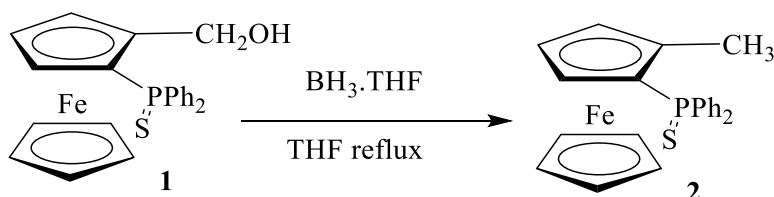
**Synthesis of Rh($\eta^3$-C$_3$H$_5$)$_3$] complex**

[Rh($\eta^3$-C$_3$H$_5$)$_3$] was prepared according to a slightly improved method from the literature.[56] A THF solution (140 mL) of RhCl$_3$.xH$_2$O (1.5 g; 7.2 mmol) was reacted with allylmagnesiumchloride (36 mL of a THF solution at 2 mol.L$^{-1}$; 71.6 mmol) under inert atmosphere and vigorous stirring at - 10°C for 1 h and then at 10°C for 16 h. During this time, the solution color changed from red to yellow. Solvent removal under reduced pressure led to a solid, which was dissolved in pentane leading to a yellow solution. After filtration through Celite, pentane was evaporated under reduced pressure and the resulting yellow solid was purified by sublimation at 40°C. Yellow crystals (660 mg, 41% yield) of [Rh($\eta^3$-C$_3$H$_5$)$_3$] were collected and stored under an argon atmosphere at low temperature. $^1$H NMR and elemental data were found identical to those from the literature.

**Synthesis of phosphino-ferrocenyl ligands**

Ligands L1 and L2,[49] L3[50] and L4[44c] were prepared according to published methods. Racemic (2-(diphenylthiophosphino)ferrocenyl)methanol (**1**) was synthesized by optimizing a literature procedure from N,N-dimethylaminomethylferrocene.[57,58]

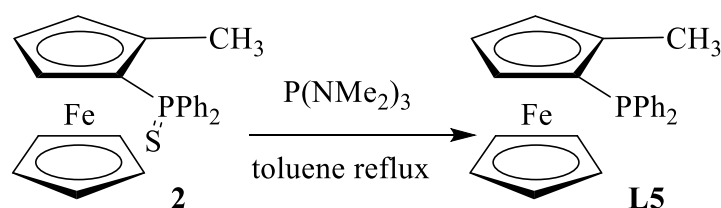**Synthesis of (2-(diphenylthiophosphino)ferrocenyl)methane 2.**

(2-(Diphenylthiophosphino)ferrocenyl)methane **2** was synthesized from alcohol **1** by adaptation of a published procedure:[59]



16

In a Schlenk tube under argon were dissolved 500 mg of alcohol **1** (1.16 mmol) in 6 mL of anhydrous THF. A BH$_3$.THF 1 M solution in THF (5 mL, 5 mmol) was then added by syringe. The reaction mixture was stirred at THF reflux for 70 h. After cooling to r.t., the Schlenk tube was opened to air and water was slowly added (warning: an abundant gas evolution occurred), leading to the formation of an orange precipitate. After THF evaporation on the vacuum line, 10 mL of dichloromethane was added for full dissolution of the orange precipitate. The remaining aqueous solution was then extracted two times with 5 mL of dichoromethane. The combined organic solutions were dried on anhydrous sodium sulfate and purified, after evaporation, by flash chromatography on silicagel using pentane/dichloromethane (50/50, v/v) as eluent to yield, after solvent evaporation, 470 mg (98% yield) of compound **2** as a yellow solid.

**$^{31}$P NMR** (162 MHz, CDCl$_3$), δ: 42.3. **$^1$H NMR** (400 MHz, CDCl$_3$), δ: 2.17 (s, 3H, CH$_3$), 3.67 (m, 1H, subst Cp), 4.22 (m, 1H, subst Cp), 4.34 (s, 5H, Cp), 4.43 (m, 1H, subst Cp), 7.35-7.55 (m, 6H, Ar), 7.63 (m, 2H, Ar), 7.81 (m, 2H, Ar). **$^{13}$C{$^1$H} NMR** (100 MHz, CDCl$_3$), δ: 14.3 (CH$_3$), 68.2 (d, $J_{C-P}$ = 10.5 Hz, subst Cp), 70.7 (s, Cp), 74.1 (d, $J_{C-P}$ = 13.2 Hz, subst Cp), 74.34 (d, $J_{C-P}$ = 96.1 Hz, quat Cp), 74.36 (d, $J_{C-P}$ = 9.9 Hz, subst Cp), 88.7 (d, $J_{C-P}$ = 12.4 Hz, quat Cp), 128.0 (d, $J_{C-P}$ = 12.4 Hz, Ar), 128.3 (d, $J_{C-P}$ = 12.4 Hz, Ar), 131.15 (d, $J_{C-P}$ = 2.6 Hz, Ar), 131.18 (d, $J_{C-P}$ = 2.6 Hz, Ar), 131.9 (d, $J_{C-P}$ = 10.9 Hz, Ar), 132.0 (d, $J_{C-P}$ = 10.5 Hz, Ar), 133.7 (d, $J_{C-P}$ = 86.0Hz, quat Ar), 134.8 (d, $J_{C-P}$ = 86.4 Hz, quat Ar). **HRMS** (ESI+) m/e: 417.0522 (M+H, 100%; calcd. for C$_{23}$H$_{22}$FePS: 417.0529).

**Synthesis of (2-(diphenylphosphino)ferrocenyl)methane L5.**



(2-(Diphenylphosphino)ferrocenyl)methane **L5** was synthesized from compound **2** by deprotection of the phosphino group following a published procedure:[60] in a Schlenk tube under argon were dissolved 470 mg of compound **2** (1.13 mmol) in 40 mL of toluene. P(NMe$_2$)$_3$ (1 mL, 5.5 mmol, 4.9 eq) was then added by syringe. The reaction mixture was stirred at toluene reflux overnight and purified by flash chromatography on silicagel under argon using pentane/dichloromethane (50/50, v/v) as eluent to yield, after solvent evaporation, 421 mg (97% yield) of compound **3** as a yellow solid.

$^{31}$P NMR (162 MHz, CDCl$_3$), δ: -21.7. $^1$H NMR (400 MHz, CDCl$_3$), δ: 2.08 (s, 3H, CH$_3$), 3.62 (m, 1H, subst Cp), 4.07 (s, 5H, Cp), 4.20 (m, 1H, subst Cp), 4.38 (m, 1H, subst Cp), 7.2-7.15 (m, 2H, Ar), 7.3-7.25 (m, 3H, Ar), 7.35-7.45 (m, 3H, Ar), 7.55-7.60 (m, 2H, Ar). $^{13}$C{$^1$H} NMR (100 MHz, CDCl$_3$), δ: 14.0 (d, $J_{C-P}$ = 10.0 Hz, CH$_3$), 68.3 (s, subst Cp), 69.7 (s, Cp), 70.4 (d, $J_{C-P}$ = 3.6 Hz, subst Cp), 72.3 (d, $J_{C-P}$ = 3.8 Hz, subst Cp), 75.7 (d, $J_{C-P}$ = 4.3 Hz, quat Cp), 89.4 (d, $J_{C-P}$ = 25.0 Hz, quat Cp), 127.8 (s, Ar), 128.14 (d, $J_{C-P}$ = 7.7Hz, Ar), 128.17 (d, $J_{C-P}$ = 5.9 Hz, Ar), 129.0 (s, Ar), 132.2 (d, $J_{C-P}$ = 18.0 Hz, Ar), 134.9 (d, $J_{C-P}$ = 20.7 Hz, Ar), 137.6 (d, $J_{C-P}$ = 8.8Hz, quat Ar), 139.7 (d, $J_{C-P}$ = 10.9 Hz, quat Ar).

**Synthesis of ferrocenylphosphine-capped Rh NPs**

In a general procedure, 150 mg of [Rh(η$^3$-C$_3$H$_5$)$_3$] (0.66 mmol) were introduced under an argon atmosphere in a Fischer-Porter reactor. After 0.5 h under vacuum at r.t. and cooling to 193 K, a CH$_2$Cl$_2$ solution (150 mL) containing 0.2 molar equivalent of the chosen ligand (L1, L2, L3 or L4) or 0.4 molar equivalent of L5 was added. The reaction medium was then allowed to warm up to r.t. before adding dihydrogen (3 bar) and then introduced in an oil bath preheated at 313 K for 16 h. After cooling to r.t., the remaining dihydrogen was vented and the volume of the solution was reduced to approximately 10 mL under reduced pressure before its transfer onto a solution of deoxygenated cold pentane (100 mL), generating the product as a black precipitate. After filtration and pentane washings the RhNPs were collected under the form of a fine powder. ICP OES analysis: for L2-stabilized RhNPs : Rh: 29.3 wt% ; for L5-stabilized RhNPs: Rh: 22.7 wt%.

## 4. Catalysis studies

In a glove-box, a Schlenk tube was charged with 12 mg of rhodium NPs. Then, 15 mL of dry degassed isopropanol and 500 µL (2.2 mmol) of dodecane (internal reference) were added to generate a stock of colloidal suspension of the catalyst. A portion of the catalyst suspension (1.5 mL) was transferred to a 5-mL glass vial (pre-charged with the desired amount of styrene or ethylbenzene substrate and NaOMe), which was then placed into a stainless steel autoclave. The reaction vessel was pressurized with 30 bar of H$_2$ and stirred with a magnetic bar for 24 h at r.t. . The reaction was stopped by release of the H$_2$ pressure and quenching with 2 mL of CH$_2$Cl$_2$, followed by filtration through silica gel. The product was finally analyzed by GC (Shimadzu 2014) using a SLB$^{TM}$ 5ms Capillary Column.

# References

[1] *Physics and Chemistry of Metal Cluster Compounds*, ed. L.J. de Jongh, Kluwer Academic Publishers, Dordrecht, 1994.

[2] Introduction to Nanotechnology*, in Nanoscale Materials in Chemistry*, ed. K.J. Klabunde, John Wiley & Sons, Inc, 2001.

[3] *Nanoparticles: From Theory to Application*, ed. G. Schmid, , Wiley-VCH, Weinheim, 2nd edn, 2012.

[4] J.E. Mondloch, E. Bayram and R.G. Finke, *J. Mol. Catal. A: Chemical*, 2012, **355**, 1-38.

[5] F. Schüth, *Angew. Chem. Int. Ed.*, 2014, **53**, 8599-8604.

[6] *Concepts in Nanocatalysis*, ed. K. Philippot and P. Serp, Wiley-VCH, Weinheim, 2013.

[7] A. Roucoux, J. Schulz and H. Patin, *Chem. Rev.*, 2002, (**102**)10, 3757–3778.

[8] *Nanocatalysis*, ed. U. Heiz and U. Landman, Springer, 2007.

[9] *Nanoparticles in catalysis*, ed. D. Astruc, Wiley-VCH, Weinheim, 2008.

[10] *Metal Nanoparticles for Catalysis: Advances and Applications*, ed. T. Tao, RSC, 2014.

[11] M.J.L. Tschan, O. Diebolt and P.W. N. M. van Leeuwen, *Top. Catal.*, 2014, **57**, 1054-1065.

[12] S. Mozaffari, W. Li, C. Thompson, S. A. Ivanov, S. Seifert, B. Lee, L. Kovarik and A. M. Karim, *Nanoscale*, 2017 (**9**)36, 13772-13785.

[13] J.E. Mondloch, S. Ozkar, R.G. Finke, *ACS Omega* 2018, (**3**)11, 14538-14550.

[14] N.J.S. Costa and L.M. Rossi, *Nanoscale*, 2012, **4**, 5826-5834.

[15] Y. Yuan, N. Yan and P.J. Dyson, *ACS Catalysis*, 2012, **2**, 1057-1069.

[16] L. Yin and M. A. El-Sayed, *J. Phys. Chem. B*, 2001, **37**, 8938-8943.

[17] R.R. Dykeman, N. Yan, R. Scopelliti and P.J. Dyson , *Inorganic chemistry*, 2011, **50**(3),717-719.

[18] D. Gonzalez-Galvez, P. Nolis, K. Philippot, B. Chaudret and P. van Leeuwen, *ACS Catalysis*, 2012, **2**(3) 317-321.

[19] S. A. Stratton, K. L. Luska and A. Moores. *Catalysis Today*, 2012, **183**(1), 96-100.

[20] H.-J. Freund and G.A. Somorjai, *Catal. Lett.*, 2015, **145**, 1-2.

[21] C. Amiens, D. Ciuculescu-Pradines and K. Philippot, *Coordination Chemistry Reviews* 2016, **308**, 409-432.

[22] Organometallic Ruthenium Nanoparticles and Catalysis, K. Philippot, P. Lignier and B. Chaudret, in *Ruthenium in catalysis 2014*, ed. C. Bruneau and P.H. Dixneuf, Wiley VCH, Weinheim, 2014, *Top. Organomet. Chem.* 2014, **48**, 319-370.

[23] PhD E. Ramírez-Meneses, University of Toulouse, 2004.

[24] S. Mavila, C. E. Diesendruck, S. Linde, L. Amir, R. Shikler and N. Gabriel Lemcoff, *Angew. Chem. Int. Ed.* 2013, **52**, 5767 –5770.

[25] E. Ramírez-Meneses, K. Philippot, M. A. Domínguez-Crespo, M. Ibrahim, I. Betancourt, A.M. Torres Huerta, A. Ezeta-Mejia and L. Palacios-Romero, *J. Mater. Sci.,* 2018, **53**(12) 8933-8950.

[26] M. Ibrahim, M. A. S. Garcia, L. Vono, M. Guerrero, P. Lecante, L. Rossi and K. Philippot, *Dalton Trans* 2016, **45**, 17782-17791.

[27] J. Llop Castelbou, E. Bresó-Femenia, P.Blondeau, B. Chaudret, S. Castillón, C. Claver and C. Godard, *Chem.Cat.Chem.* 2014, **6**, 3160- 3168.

[28] M.A.S. Garcia, M. Ibrahim, J.C. S. Costa, P. Corio, E.V. Gusevskaya, E.N. dos Santos, K. Philippot and L. M. Rossi, *Applied Catalysis A*, 2017, **548**, 136-142.

[29] K. M. Roth, A.A. Yasseri, Z. Liu, R. B. Dabke, V. Malinovskii, K.-H.Schweikart, L. Yu, H. Tiznado, F. Zaera, J. S. Lindsey, W. G. Kuhr and D. F. Bocian, J. *Am. Chem. Soc.*, 2003, **125**(2), 505–517.

[30] X. Su and T. A. Hatton, *Advances in Colloid and Interface Science*, 2017, **244**, 6–20.

[31] J. De Tovar, N. Romero, S. Denisov, R. Bofill, C. Gimbert-Suriñach, D. Ciuculescu-Pradines, S. Drouet, A. Llobet, P. Lecante, V. Colliere, Z. Freixa, N. McClenaghan, C. Amiens, J. García-Antón, K. Philippot and X. Sala, *Materials Today Energy*, 2018, **9**, 506-515.

[32] G. G. A. Balavoine, J.-C. Daran, G. Iftime, P. G. Lacroix, E. Manoury, J. A. Delaire, I. Maltey-Fenton, K. Nakatani andS. Di Bella, *Organometallics*, 1999 (18) 21-29.

[33] W. Chen, H.-U. Blaser, in Phosphorus Ligands in Asymmetric Catalysis ed. by A. Börner,Wiley-VCH, Weinheim, **2008,** 345-359.

[34] R. Gómez Arrayás, J. Adrio and J. C. Carretero, *Angew. Chem. , Int. Ed. Engl.* 2006 (**45**) 7674-7715.

[35] S. Toma, J. Csizmadiova, M. Meciarova and R. Sebesta, *Dalton Trans.* 2014 (**43**) 16557–16579

[36] V. Blanco, D. A. Leigh and V. Marcost, *Chem. Soc. Rev.* 2015 (**44***)* 5341-5370.

[37] A. Feyrer, M. K. Armbruster, K. Fink and F. Breher, *Chem. Eur. J.* **2017** (**23**) 7402-7408.

[38] J. Choudhury, *Tet. Lett.* 2018 (**59**) 487-495.

[39] T. J. Colacot, *Chem. Rev.* 2013(103) 3101-3118.

[40] H. A. McManus and P. J. Guiry, *Chemical Reviews* 2004 (**104**) 4151-4202.

[41] M. Mellah, A. Voituriez and E. Schulz, *Chem. Rev.*, 2007 (**107**) 5133-5209.

[42] H. Pellissier, *Tetrahedron*, 2007 (**63**) 1297-1330.

[43] R. Malacea, E. Manoury, in "Phosphorus Ligands in Asymmetric Catalysis" edited by Armin Börner (Wiley-VCH, Weinheim, Germany), 2008**,**. 749-784.

[44] N. Mateus, L. Routaboul, J.-C. Daran, and E. Manoury, *J.Organomet. Chem.* 2006 (**691**) 2297-2310.

[45] C. Audin, J.-C. Daran, E. Deydier, E. Manoury and R. Poli, *CR Chimie* 2010 (**13**) 890-899.

[46] S. Bayda, A. Cassen, J.-C. Daran, C. Audin, R. Poli, E. Manoury and E. Deydier, *J. Organomet. Chem.,* 2014 (**772-773**) 258-264.

[47] A. Karpus, O. Yesypenko, V. Boiko, R. Poli, J.-C. Daran, Z. Voitenko, V. Kalchenko and E. Manoury, *Eur. J. Org. Chem.*, 2016 (**20**) 3386-3394.

[48] K. Yoshida and R. Yasue, *Chem. Eur. J.* 2018 (**24***)* 18575- 18586.

[49]M.-M. Wei, M. García-Melchor, A. Lledós, C. Audin, J.-C. Daran, R. Poli, E. Deydier and E. Manoury, *Organometallics,* 2012 (**31**) 6669-6680.

[50] L. Routaboul, S. Vincendeau, J.-C. Daran and E. Manoury, *Tetrahedron Asym.*, 2005 (**16**) 2685-2690.

[51] R. Choukroun, D. de Caro, B. Chaudret, P. Lecante and E. Snoeck, New J. Chem., 2001 (**25**) 525–527.

[52] F. Novio, D. Monahan, Y. Coppel, G. Antorrena, P. Lecante, K. Philippot and B. Chaudret, *Chemistry*: *A Eur. J.,* 2014 (**20**)5, 1287-1297.

[53] PhD M. Ibrahim, Université fédérale de Toulouse- Paul Sabatier, 2016.

[54] J.S. Bradley, J.M. Millar, E.W. Hill and S. Behal, *Journal of Catalysis*, 1991 (**129**) 530-539.

[55] J.S. Bradley, J.M. Millar, E.W. Hill, S. Behal, C. Klein, A. Duteil and B. Chaudret, *Chem. Mater.* 1992 (**4**) 1234-1239.

[56] R. Beckhaus, in *Synthetic Methods of Organometallic and Inorganic Chemistry*, Vol. 9, ed. W.A. Herrmann, New York, 2000, 38.

[57] T. Hayashi, T. Mise, M. Fukushima, M. Kagotani, N. Nagashima, Y. Hamada, A. Matsumoto, S. Kawakami, M. Konishi, K. Yamamoto and M. Kumada, *Bull. Chem. Soc. Jpn.*, 1980 (**53***)* 1138-1151.

[58] E. Manoury, and R. Poli, in the Series: *Catalysis by Metal Complexes* (CMCO), Volume 36 (Phosphorus Chemistry: Catalysis and Material Science Applications), ed. M. Peruzzini and L. Gonsalvi,Springer Verlag, 2011 (**36**) 121-149.

[59] L. Routaboul, J. Chiffre, G.G.A. Balavoine, J.-C. Daran and E. Manoury, E., *J. Organomet. Chem.*, 2001, (**637-639**) 364-371.

[60] J. Lopez Cortes, O. Ramon, S. Vincendeau, D. Serra, F. Lamy, J.C. Daran, E. Manoury and M. Gouygou, *Eur. J. Inorg. Chem.*, 2006 (**24**) 5148-5157.